01 Jan 1974

Hybrid Carrier And Modulation Tracking Loop Performance In RFI

Rodger E. Ziemer

Missouri University of Science and Technology

Donald R. Nelson

Recommended Citation

R. E. Ziemer and D. R. Nelson, "Hybrid Carrier And Modulation Tracking Loop Performance In RFI," *IEEE Transactions on Communications*, vol. 22, no. 10, pp. 1607 - 1617, Institute of Electrical and Electronics Engineers, Jan 1974.

The definitive version is available at https://doi.org/10.1109/TCOM.1974.1092084

Hybrid Carrier and Modulation Tracking Loop Performance in RFI

RODGER E. ZIEMER, SENIOR MEMBER, IEEE, AND DONALD R. NELSON, MEMBER, IEEE

Abstract—The operation of a hybrid tracking (HT) phase-locked loop (PLL) in radio-frequency interference (RFI) is considered. Results from a perturbation analysis for the loop phase error in continuous-wave (CW) RFI are found to compare favorably with results obtained by digital computer simulation. These results, together with simulation results for wide-band (in comparison to the loop bandwidth) RFI, indicate that loop structures which track both on the signal carrier and modulation components are advantageous in RFI plus Gaussian noise backgrounds.

INTRODUCTION

Of considerable interest and importance in many applications is the effect of radio-frequency interference (RFI) on communication systems. Possible applications include the use of synchronous-orbit relay satellites for communication between low-flying users, such as other satellites or aircraft, and ground stations. Typical users in such links are low power and have antennas with little directivity. As such, interference levels at the users, due to earth-based sources, may be comparable to signal levels.

In this paper, the effect of RFI on the performance of a hybrid tracking (HT) loop is examined. Hybrid carrier and modulation tracking loops, as considered by Lindsey [1] and others [2], [3], make use of both the carrier and sideband components of a digitally phase-modulated signal to establish a coherent reference. Previous investigations have indicated that modulation tracking loops may tolerate cochannel RFI better than carrier tracking loops [4]. Here a perturbation solution for the phase error in an HT loop due to continuous-wave (CW) RFI alone, and simulation results for both RFI and noise backgrounds are used to characterize HT loop performance in RFI. The results show that modulation tracking loops can give improved performance in RFI over carrier tracking loops.

EQUATIONS OF OPERATION

In Fig. 1, the block diagram of a simplified HT loop is shown. As pointed out by Lindsey [1], this is only one of several possible equivalent configurations.

Paper approved by the Associate Editor for Data Communication Systems of the IEEE Communications Society for publication after presentation at the National Telemetering Conference, Houston, Tex., 1972. This work was supported by NASA Goddard Space Flight Center, Greenbelt, Md., under Contract NAS-5-20282. Manuscript received March 20, 1974; revised June 13, 1974.

R. E. Ziemer is with the Department of Electrical Engineering, University of Missouri-Rolla, Rolla, Mo.

D. R. Nelson is with the Department of Computer and Digital Equipment, Aerospace Corporation, El Segundo, Calif.

Let the input to the system of Fig. 1 consist of a binary phase-modulated signal plus noise

$$x(t) = s_k(t) + n(t) \tag{1}$$

where

$$s_k(t) = (2P)^{1/2} \sin [\omega_0 t + \theta(t) + x_k(t) \cos^{-1} m], \qquad t_0 \le t \le t_0 + T_b,\ k = 0,1, \tag{2}$$

represents the signal component, and

$$n(t) = n_g(t) + n_{\mathrm{CW}}(t) + n_{wb}(t) = \sqrt{2}[n_c(t) \cos (\omega_0 t + \theta) + n_s(t) \sin (\omega_0 t + \theta)] \tag{3}$$

represents the noise component. In (3) n_g, n_{CW}, and n_{wb} are band-limited white Gaussian noise, CW interference, and wide-band (in comparison to the loop bandwidth) interference, respectively. Rewriting (2), as the sum of carrier and modulation components, yields

$$s_k(t) = (2P)^{1/2} m \sin (\omega_0 t + \theta) + (2P)^{1/2}(1 - m^2)^{1/2} \cdot x_k(t) \cos (\omega_0 t + \theta)] \tag{4}$$

where

P	average signal power,
ω_0	carrier frequency (rad/s),
m^2	fraction of power in carrier component,
θ	RF phase (rad), and
$x_k(t)$	the modulation which consists of sequences of $\pm$ 1's in T_b-second intervals.

Here, $x_k(t)$ is taken as data $d_k(t)$, placed on a subcarrier of ω_{sc} rad/s.

Choosing a loop filter of the form

$$F(p) = \frac{p + a}{p + \epsilon}, \tag{5}$$

where p is the differential operator d/dt, and ϵ is the loop imperfection factor, the loop differential equation can be derived in a straightforward fashion. It is convenient to write this differential equation in terms of normalized time

$$\tau = 2\zeta\omega_n t \tag{6}$$

where

$$\omega_n = (G_0 a)^{1/2}, \tag{7}$$

$$\zeta = \frac{1}{2} \frac{G_0 + \epsilon}{(G_0 a)^{1/2}}, \tag{8}$$

and

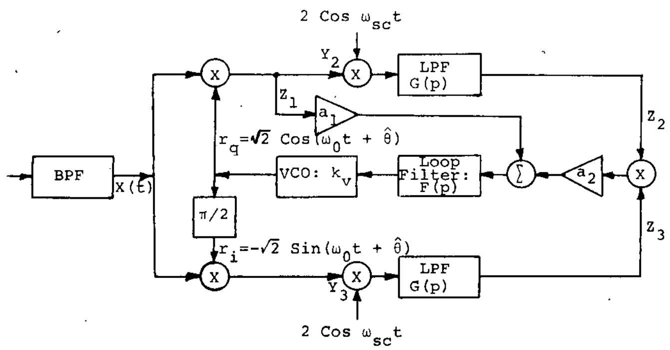

Fig. 1. Hybrid loop block diagram.

$$G_0 = k_v[a_1 m P^{1/2} + a_2(1 - m^2)P]. \tag{9}$$

In (9), k_v is the voltage-controlled oscillator (VCO) constant (rad/s/V) and the other parameters not defined previously are defined in Fig. 1. The parameters ζ and ω_n are the damping factor and natural frequency of the linearized loop, respectively. Expressed in terms of τ, the loop differential equation in normal form is shown in the Appendix to be

$$\dot{\phi}(\tau) = y(\tau) - \frac{1}{(1+\epsilon_n)} \frac{F(\tau;\phi)}{[m + \rho(1-m^2)]} + \dot{\theta}(\tau)$$

$$\dot{y}(\tau) = -\frac{\epsilon_n}{(1+\epsilon_n)} y(\tau) + \left[\frac{\epsilon_n}{(1+\epsilon_n)^2} - \frac{1}{4\zeta^2}\right] \cdot \frac{F(\tau;\phi)}{[m + \rho(1-m^2)]} \tag{10}$$

where $\phi = \theta - \hat{\theta}$ is the phase error, the dot denotes differentiation with respect to τ, $\epsilon_n = \epsilon/G_0$, and

$$\rho \triangleq a_2 P^{1/2}/a_1 \tag{11}$$

is the ratio of the low-frequency gain of the modulation tracking loop to that of the carrier tracking loop.

The function $F(\tau;\phi)$, which contains the signal and noise dependent terms, can be written as

$$F(\tau;\phi) = (Z_1 + \rho Z_2 Z_3/P^{1/2})/P^{1/2} \tag{12}$$

where

$$Z_1(\tau) = [mP^{1/2} + n_s(\tau)] \sin\phi + n_c(\tau)\cos\phi \tag{13}$$

and Z_2 and Z_3 are the result of passing Y_2 and Y_3 (see Fig. 1) through the low-pass filters with transfer functions $G(p)$ after multiplication by $2\cos\omega_{sc}t$. Assuming $G(p)$ to have bandwidth much wider than the loop bandwidth (say, wide enough to pass $d_k(\tau)$ with negligible distortion), it follows that Z_2 and Z_3 may be written as

$$Z_2(\tau) = [G(p)d_k(\tau)P^{1/2}(1-m^2)^{1/2} + n_1(\tau)]\cos\phi + n_2(\tau)\sin\phi \tag{14}$$

$$Z_3(\tau) = [G(p)d_k(\tau)P^{1/2}(1-m^2)^{1/2} + n_1(\tau)]\sin\phi - n_2(\tau)\cos\phi \tag{15}$$

where $n_1(\tau)$ and $n_2(\tau)$ are the quadrature noise components in the modulation tracking portion of the loop. (It is tacitly assumed that frequencies are scaled in accordance with (6), also.) From Fig. 1 and (3), it follows that

$$n_1(\tau) = G(p)[n_c(\tau)\cdot 2\cos(\omega_{sc}/2\zeta\omega_n)\tau] \tag{16}$$

and

$$n_2(\tau) = G(p)[n_s(\tau)\cdot 2\cos(\omega_{sc}/2\zeta\omega_n)\tau]. \tag{17}$$

Assuming, for the moment, that $n(t)$ is composed of white Gaussian noise alone with two-sided spectral density $N_0/2$, then n_1 and n_2, the quadrature noise components in the modulation tracking loop, and n_c and n_s, the quadrature noise components in the phase-locked loop (PLL), are of wide bandwidth compared to the loop bandwidth. As a result, they can also be considered white with spectral density $N_0/2$. They are mutually independent since n_1 and n_2 are quadrature components as are n_c and n_s; also, n_1 and n_2 occupy a spectral region which is disjoint from that occupied by n_c and n_s. In the τ-domain, the spectral density of these noise components becomes $\zeta\omega_n N_0$.

Lindsey [1] and others have considered the case of white Gaussian noise corrupting the input signal. The remainder of this paper will be concerned with the effect on loop operation of RFI whose bandwidth is small (CW case) or large (wide-band case) in comparison to the loop bandwidth.

PERTURBATION ANALYSIS OF CW RFI

The effect of a CW RFI component of the form

$$\begin{aligned} n_{CW}(t) &= (2\alpha)^{1/2}\cos[(\omega_0 - \Delta\omega)t + \theta - \delta] \\ &= (2\alpha)^{1/2}\cos(\Delta\omega t + \delta)\cos(\omega_0 t + \theta) \\ &\quad + (2\alpha)^{1/2}\sin(\Delta\omega t + \delta)\sin(\omega_0 t + \theta) \end{aligned} \tag{18}$$

at the loop input in the absence of Gaussian noise can be approximated by means of a simple perturbation analysis. In (18), α^2 is the interference power, $\Delta\omega$ the radian frequency offset of the RFI from the signal frequency, and δ the phase of the interference relative to the signal phase θ. Defining the RFI phase δ such that θ, the relative signal phase, is its reference, allows the loop differential equation for CW RFI to be obtained simply by replacing $n_c(\tau)$ and $n_s(\tau)$ in (13), (16), and (17) by $\alpha\cos[(\Delta\omega/2\zeta\omega_n)\tau + \delta]$ and $\alpha\sin[(\Delta\omega/2\zeta\omega_n)\tau + \delta]$, or in the t-domain, by $\alpha\cos(\Delta\omega t + \delta)$ and $\alpha\sin(\Delta\omega t + \delta)$, respectively. To avoid factors of $2\zeta\omega_n$, the analysis for CW RFI will be carried out in the t-domain.

In the Appendix, it is shown that if the interference-to-signal ratio is small, the effect of RFI on the operation of the loop obeys the equation

$$\phi = -H(p)R(t;\phi) \tag{19}$$

where

$$H(p) = \frac{2\zeta\omega_n p + \omega_n^2}{p^2 + 2\zeta\omega_n p + \omega_n^2} \tag{20}$$

is the closed loop transfer function of the linearized loop,

$p = d/dt$ and $\epsilon_n = 0$ has been assumed. The RFI forcing function, $R(t;\phi)$, is shown in the Appendix to be given by

$$R(t;\phi) = [m + \rho(1 - m^2)]^{-1}[I \cos(\phi - \gamma_1) + \epsilon_x\rho(1 - m^2)^{1/2}d_k(t)IB_- \sin(2\phi - \gamma_2) + \tfrac{1}{2}\rho I^2 B_-^2 \sin 2(\phi - \gamma_2)] \quad (21)$$

where ϵ_x will be defined shortly, and

$$I = \alpha/P^{1/2} \quad (22)$$

is the interference-to-signal ratio at the loop input. The transfer function of the in-phase and quadrature channel filters has been represented as

$$G(j\omega) = B(j\omega) \exp[j\psi(j\omega)], \quad (23)$$

where $B(j\omega)$ is the amplitude response and $\psi(j\omega)$ is the phase response. To simplify notation,

$$\gamma_1 = \Delta\omega t + \delta, \quad (24a)$$

$$\gamma_2 = (\Delta\omega - \omega_{sc})t - \delta + \psi(\Delta\omega - \omega_{sc}), \quad (24b)$$

and

$$B_- = B(\Delta\omega - \omega_{sc}) \quad (25)$$

have been introduced.

Two extremes can be considered for the data rate T_b^{-1}, relative to the offset frequency of the interference in the loop passband, $(\Delta\omega - \omega_{sc})/2\pi$. First, if $T_b^{-1} \ll (\Delta\omega - \omega_{sc})/2\pi$, i.e., low data rate relative to the interference offset frequency, $d_k(t)$ in (19) can be replaced by unity since the data are constant over many cycles of the interference. Second, if $T_b^{-1} \gg (\Delta\omega - \omega_{sc})/2\pi$, i.e., high data rate relative to the interference offset frequency, a rough idea of how the loop will respond is obtained by noting that the interference factor in the fourth term of (19) is a quantity that is slowly varying relative to the bit rate. Assuming $E[d_k(t)] = 0$, the filtering by the closed loop system will effectively cause the (modulation) $\times$ (interference) term to average to zero in (21). Thus, one would expect that the effect of the interference in such a situation would be smaller than for the low data-rate case. To treat the crossterm in this fashion is, of course, an oversimplification, but simulation results bear this conjecture out [4]. Thus, parameter ϵ_x is defined as

$$\epsilon_x = \begin{cases} 1, & T_b^{-1} \ll (\Delta\omega - \omega_{sc})/2\pi \quad \text{(low data rate)} \\ 0, & T_b^{-1} \gg (\Delta\omega - \omega_{sc})/2\pi \quad \text{high data rate)} \end{cases} \quad (26)$$

in accordance with the discussion above.

A series solution is now obtained to (19) by the variation-iteration method [5]. The zeroth-order approximation ϕ_0 is obtained by letting $\phi = 0$ on the right side of (19). The result is

$$\phi_0(t) = -|H(\Delta\omega)|[m + \rho(1 - m^2)]^{-1}[I \cos(\gamma_1 + \angle H(\Delta\omega)) - \epsilon_x\rho(1 - m^2)^{1/2}IB_- \cdot \sin(\gamma_2 + \angle H(\Delta\omega))] + \tfrac{1}{2}\rho|H(2\Delta\omega)|[m + \rho(1 - m^2)]^{-1}I^2B_-^2 \cdot \sin(2\gamma_2 + \angle H(2\Delta\omega)) \quad (27)$$

where $|H|$ and $\angle H$ are the amplitude and phase response of the closed loop system, respectively. The first-order approximation is obtained by substituting (27) on the right side of (19) after using the approximations $\cos \phi_0 = 1$ and $\sin \phi_0 = \phi_0$. Since $T_b^{-1} \gg (\Delta\omega - \omega_{sc}/2\pi)$ is the case of most interest, attention will be restricted to it for the first-order approximation. Letting $\epsilon_x = 0$ in (21) and (27), and keeping terms of second order or less in I, the result is

$$\phi_1(t) = B_0 + B_1 \cos(\Delta\omega t + \delta + \angle H(\Delta\omega)) + B_2 \cos(2\Delta\omega t + 2\delta + \angle(2\Delta\omega)) + B_3 \sin(2\Delta\omega t + 2\delta + \angle H(2\Delta\omega)) \quad (28)$$

where

$$B_0 = \tfrac{1}{2}I^2|H(\Delta\omega)|[m + \rho(1 - m^2)]^{-2}, \quad (29)$$

$$B_1 = -I|H(\Delta\omega)|[m + \rho(1 - m^2)]^{-1}, \quad (30)$$

$$B_2 = -\tfrac{1}{2}I^2|H(2\Delta\omega)|[m + \rho(1 - m^2)]^{-2} \cdot \{|H(\Delta\omega)| \sin \angle H(\Delta\omega) + \rho B_-^2[m + \rho(1 - m^2)] \cdot \sin 2\psi(\Delta\omega - \omega_{sc})\}, \quad (31)$$

and

$$B_3 = -\tfrac{1}{2}I^2|H(2\Delta\omega)|[m + \rho(1 - m^2)]^{-2} \cdot \{|H(\Delta\omega)| \cos \angle H(\Delta\omega) + \rho B_-^2[m + \rho(1 - m^2)] \cos 2\psi(\Delta\omega - \omega_{sc})\}. \quad (32)$$

Since (28) is a sum of harmonics, an approximation for the phase error variance is given by one-half of the sum of the squares of the last three terms, i.e.,

$$\hat{\sigma}_\phi^2 = \tfrac{1}{2}(B_1^2 + B_2^2 + B_3^2). \quad (33)$$

An approximation for the mean-square phase error is given by

$$\widehat{\overline{\phi^2}} = B_0^2 + \hat{\sigma}_\phi^2 \quad (34)$$

since B_0 is the mean of the phase error. Results calculated from (33) and (34) are compared with simulation results in Figs. 2–4.

Although the effects of Gaussian noise were not included in the preceding analysis, and to do so would be difficult, it seems reasonable that the phase error components due to the effects of Gaussian noise and CW interference could be assumed additive at high signal-to-interference-plus-noise ratios (SINR's). This follows if the (noise) $\times$ (interference) terms in the loop control voltage are small relative to the noise or interference terms alone. Since the (noise) $\times$ (interference) interaction is a second-order effect in SINR^{-1}, additivity is a reasonable assumption for large SINR's.

EFFECT OF RFI WITH BANDWIDTH COMPARABLE TO THE SIGNAL BANDWIDTH

In addition to CW RFI, the effect of RFI representative of modulated interfering-signal sources is also of interest. For such RFI sources, the interfering signal at the loop

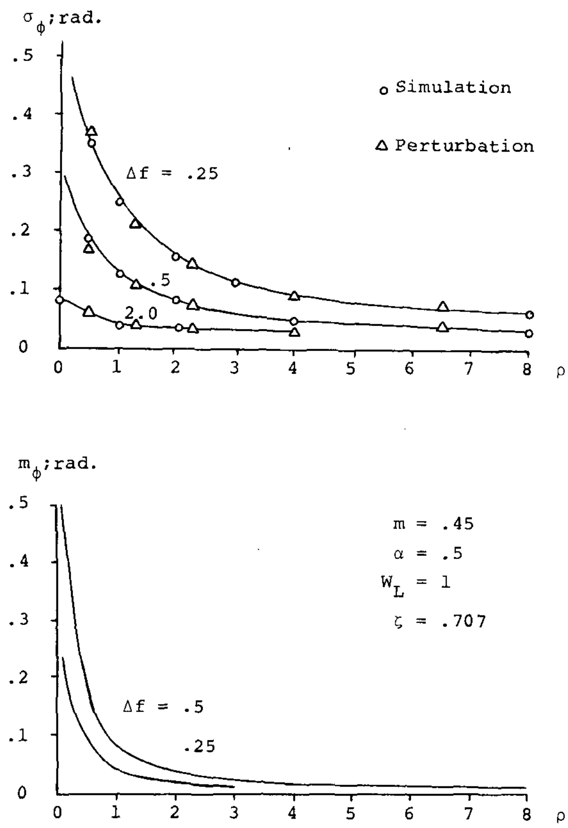

Fig. 2. Phase error standard deviation and mean for CW RFI; $m = 0.45$.

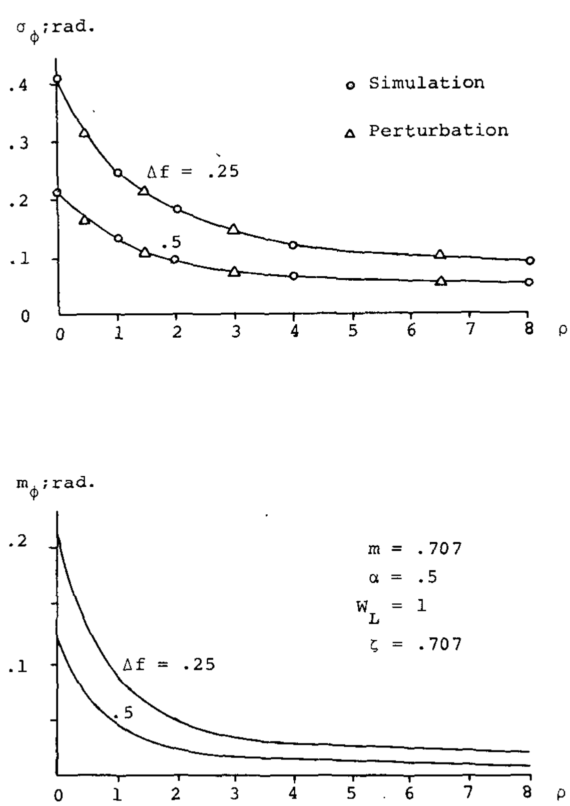

Fig. 3. Phase error standard deviation and mean for CW RFI; $m = 0.707$.

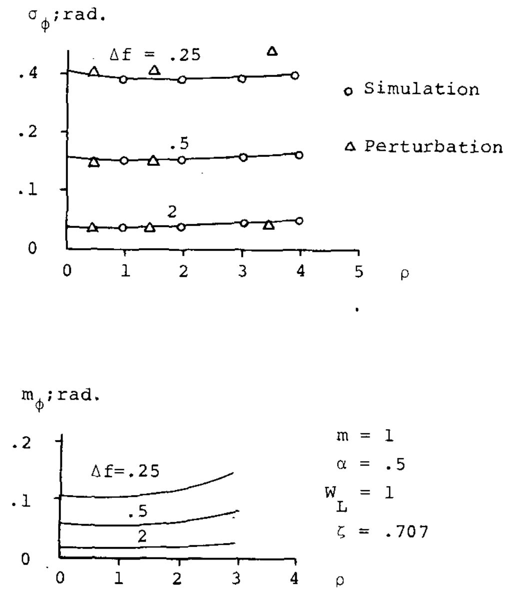

Fig. 4. Phase error standard deviation and mean for CW RFI; $m = 1$.

input is represented as

$$n_{wb}(t) = \sqrt{2}R(t) \cos[(\omega_0 - \Delta\omega_2)t + \theta - \delta_2] \quad (35)$$

where $R(t)$ is a Rayleigh random process and δ_2 a uniform random variable. Equation (35) can be expanded as

$$\begin{aligned} n_{wb}(t) &= \sqrt{2}[R(t) \cos(\Delta\omega_2 t + \delta_2) \cos(\omega_0 t + \theta) \\ &\quad + R(t) \sin(\Delta\omega_2 t + \delta_2) \sin(\omega_0 t + \theta)] \\ &= \sqrt{2}[n_{cwb}(t) \cos(\omega_0 t + \theta) + n_{swb}(t) \\ &\quad \cdot \sin(\omega_0 t + \theta)] \end{aligned} \quad (36)$$

where

$$\begin{aligned} n_{cwb}(t) &= R(t) \cos\delta_2 \cos\Delta\omega_2 t - R(t) \sin\delta_2 \sin\Delta\omega_2 t \\ &= n_{cg}(t) \cos\Delta\omega_2 t - n_{sg}(t) \sin\Delta\omega_2 t, \end{aligned} \quad (37a)$$

$$\begin{aligned} n_{swb}(t) &= R(t) \sin\delta_2 \cos\Delta\omega_2 t + R(t) \cos\delta_2 \sin\Delta\omega_2 t \\ &= n_{sg}(t) \cos\Delta\omega_2 t + n_{cg}(t) \sin\Delta\omega_2 t. \end{aligned} \quad (37b)$$

The random processes $n_{cg}(t)$ and $n_{sg}(t)$ are low-pass Gaussian. Comparing (36) with (3), it is apparent that the inclusion of $n_{wb}(t)$ in the equations describing the loop operation is accomplished by replacing $n_c(t)$ and $n_s(t)$ in (13), (16), and (17) by $n_{cwb}(t)$ and $n_{swb}(t)$, respectively (or $n_c + n_{cwb}$ and $n_s + n_{swb}$ if the effect of white Gaussian noise plus interference is desired). Unfortunately, a simple analysis, such as the perturbation analysis for CW RFI, appears impossible for wide-band RFI. Thus, loop operation in the presence of noise and RFI was simulated.

COMPUTER SIMULATION

The loop differential equations (10) are integrated numerically in response to the forcing function $F(\tau,\phi)$. The modulation, $d_k(t)$, is a 63-bit maximal-length pseudonoise sequence. However, any sequence capable of being generated by a single feedback shift register is possible with the subroutine used in the simulation. $\theta(t)$ is selected to represent a constant offset frequency of Ω_0 rad/s. For the simulation results presented here, $\Omega_0 = 0$. CW RFI is simulated simply by letting α and δ be constants in (18). Alternatively, δ can be chosen as a sample function from a Wiener process. Wide-band RFI is simulated by generating low-pass Gaussian time series with autocorrelation function

$$R(\sigma) = A \exp[-2\pi W|\sigma|],$$

where W is the 3-dB bandwidth of the process, by using Levin's method [6]. The modulation-tracking loop filters, $G(p)$, are selectable as first-through fourth-order Butterworth. Second-order filtering is used to obtain the results presented in this paper.

RESULTS AND DISCUSSION OF RESULTS

CW RFI

Results from the perturbation analysis and simulation for the phase error standard deviation (i.e., the square root of (33) and mean of the phase error (i.e., B_0) are compared as functions of ρ in Figs. 2–4 for $m = 0.45$, 0.707, and 1. This corresponds to 20, 50, and 100 percent of the transmitted signal power in the carrier component, respectively. A damping factor of $\zeta = 0.707$ is assumed, and the in-phase and quadrature channel filters are second-order Butterworth with normalized cutoff frequency equal to 12 Hz. The double-sided loop bandwidth is 1 Hz which, in effect, means that the results have been normalized by W. Other parameter values are $\epsilon_n = 5 \times 10^{-4}$, $2\zeta\omega_n = 1.33$, and $T_b = 0.1667$.

In Figs. 5–7, rms phase error is shown as a function of $\beta = \Delta\omega/2\zeta\omega_n$ for $\zeta = 0.707$ and several values of ρ. Recalling the definition of ρ [see (11)], Figs. 5–7 clearly show the desirability of modulation tracking loops (large ρ) in CW RFI backgrounds provided, of course, that significant power in the received signal is allocated to the modulation component.

As an indication of how the character of the phase error pdf changes with ρ, Fig. 8 shows histogram approximations to the phase error pdf for $\rho = 0.25$, 0.5, 1, and 4. Note that the scale on the abscissa varies from one figure to the next. Fig. 8(d) corresponds to the smallest phase error variance. The tendency of the phase error pdf toward a Gaussian shape as ρ increases is clearly evident. This is apparently due to the switching effect of the data stream on the (data) $\times$ (interference) components of the loop control voltage and the subsequent filtering by the loop.

CW Interference Plus Gaussian Noise

As a somewhat more realistic environment, simulations for loop operation in a CW interference plus white Gaussian noise background were carried out. Results are presented here which characterize loop operation in both the threshold region and above threshold.

1) *Mean Time to First Slip*: Shown in Fig. 9 are simulation results for normalized mean time to first slip as a function of signal-to-noise ratio. The same parameter values were used as for the simulations for CW RFI without noise. The presence of interference in addition to the noise lowers the mean time to slip. When operation is closer to a PLL mode ($\rho = 0$) than a modulation tracking mode ($\rho = 0.75$), the threshold is higher. This is attributed to the domination of the (noise) $\times$ (noise) terms in the

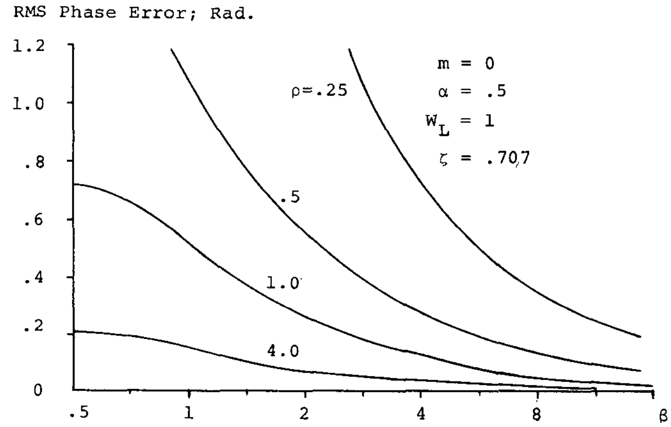

Fig. 5. rms phase error versus β for $m = 0$.

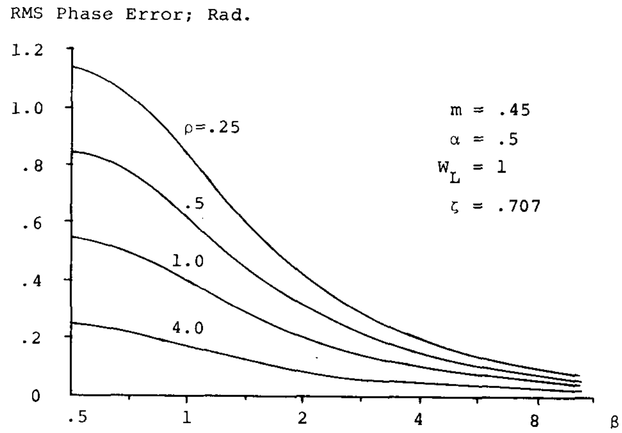

Fig. 6. rms phase error versus β for $m = 0.45$.

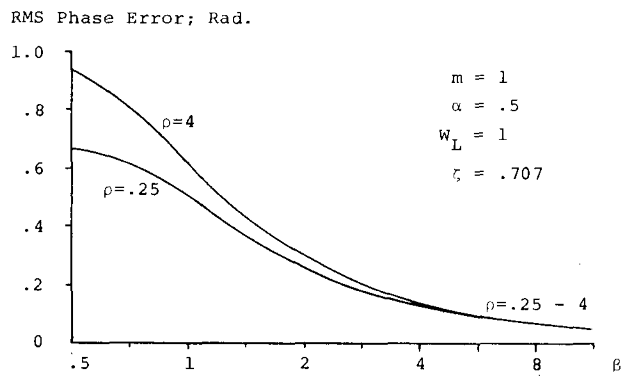

Fig. 7. rms phase error versus β for $m = 1$.

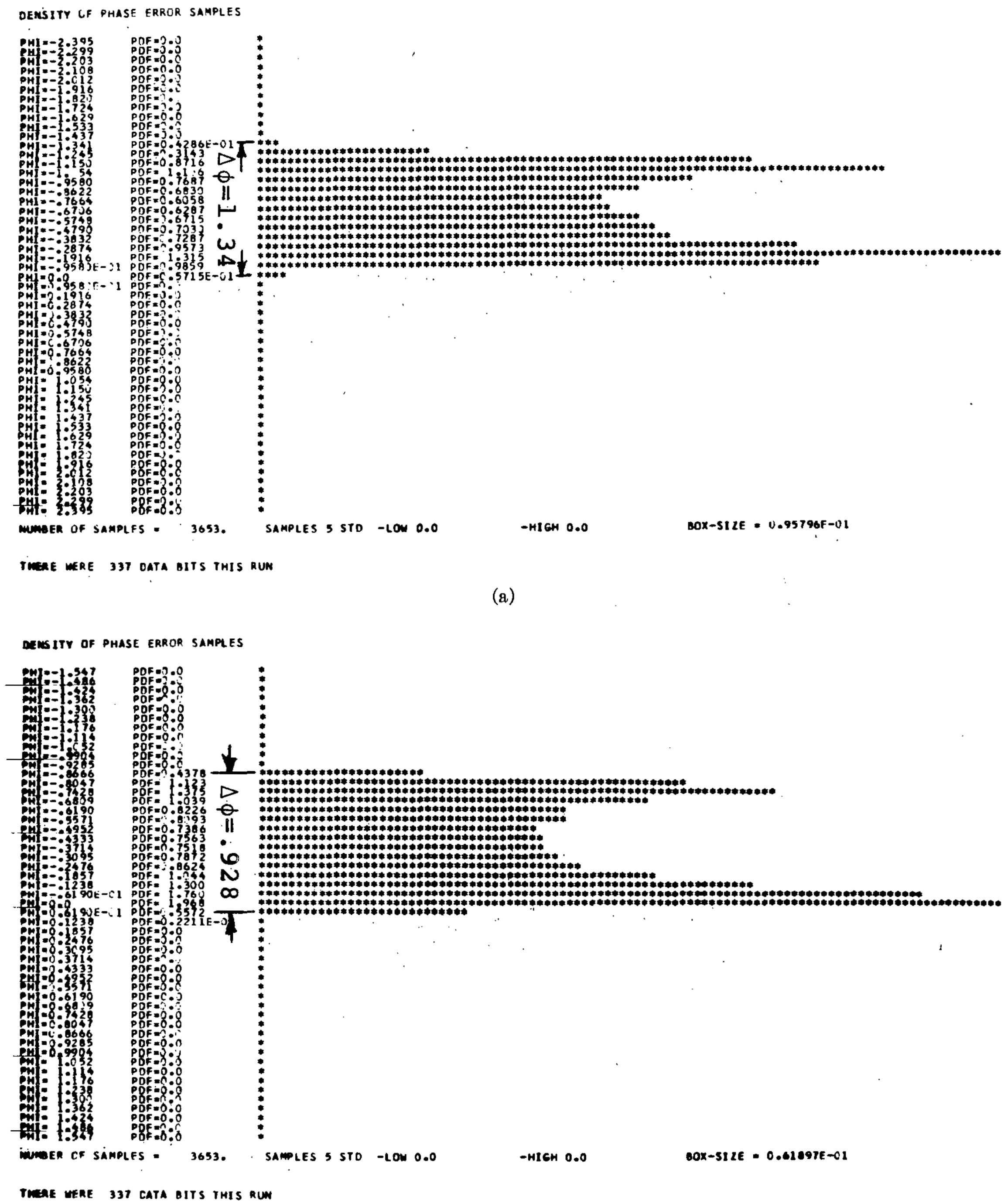

(a)

(b)

Fig. 8. Histogram approximation for phase error pdf. (a) $\alpha = 1.1$, $\Delta f = 0.667$, $\rho = 0.25$. (b) $\alpha = 1.1$, $\Delta f = 0.667$, $\rho = 0.5$.

loop control voltage at low signal-to-noise ratios for ρ nonzero.

It should also be remembered that $m = 0.45$ corresponds to 80 percent of the transmitted power in the modulation, and the remaining power in the carrier. In the PLL mode ($\rho = 0$) tracking must be on the carrier component alone. However, $m = 1$ for $\rho = 0$ is not a fair basis of comparison with $m = 0.45$ and $\rho = 0.75$. A fairer basis of comparison would be $m = 0.45$ with $\rho = 0$ which would correspond to PLL tracking of a phase-shift-keyed signal with 80 percent of the power in the sidebands. The result is shown as dashed curves in Fig. 9. Even with this adjustment, the threshold for the PLL mode is below that for the hybrid mode. For another value of ρ, however, this may not be the case. Extensive simulations for threshold characterization are not presented because they are extremely time consuming to simulate.

2) *Phase Error Variance and Probability of Error*: Above

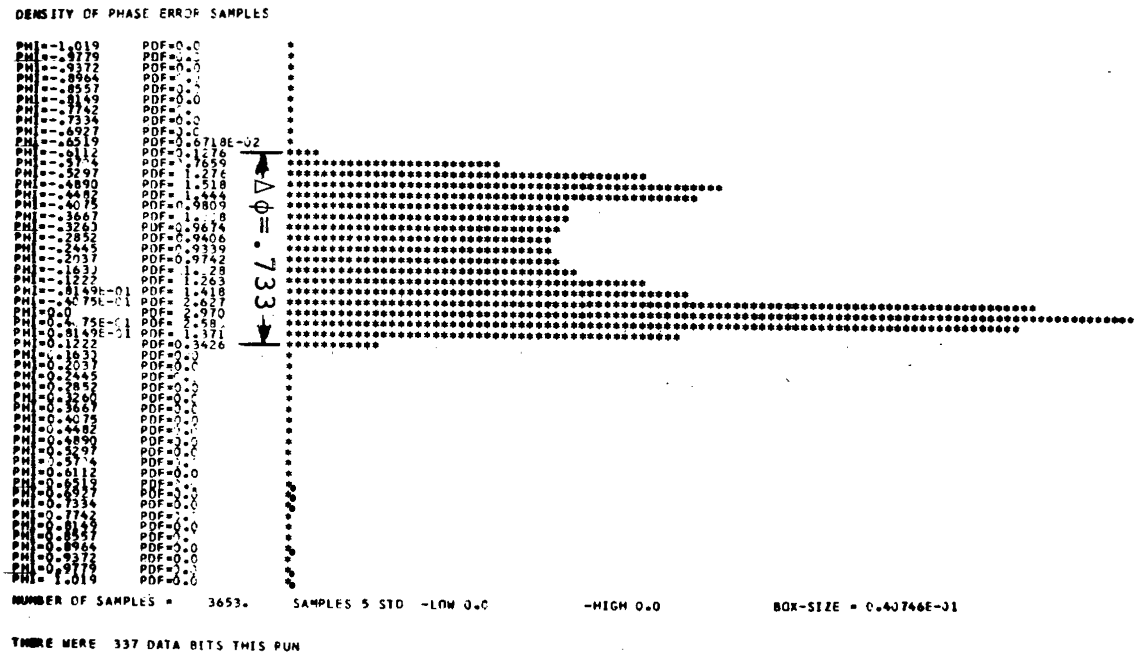

(c)

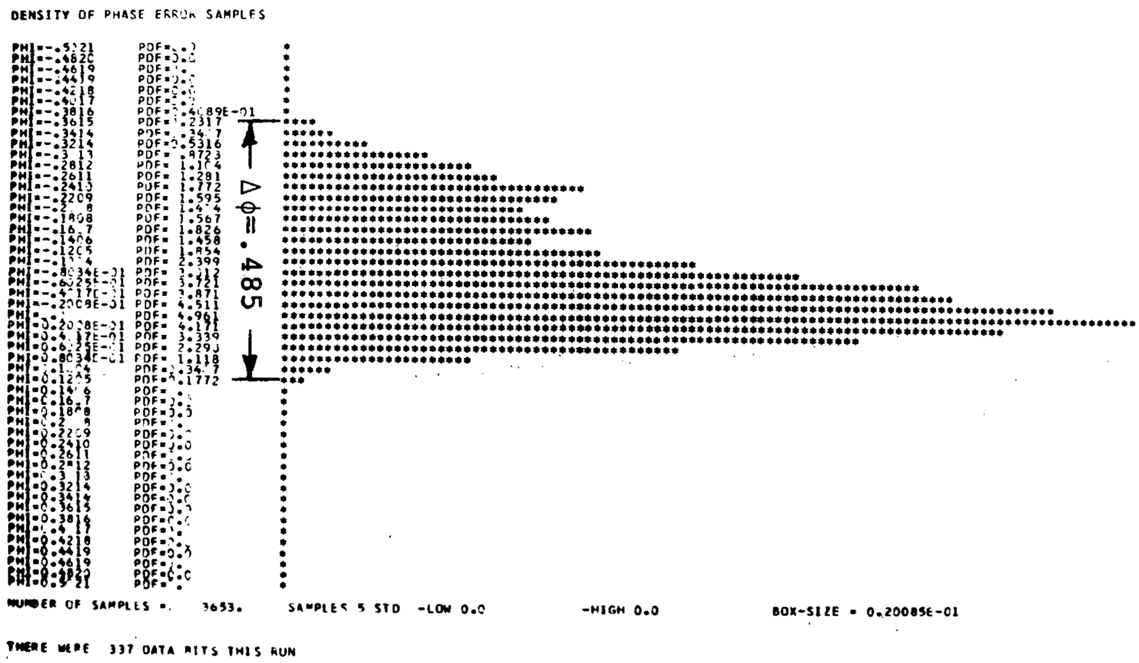

(d)

Fig. 8 (continued). (c) $\alpha = 1.1$, $\Delta f = 0.667$, $\rho = 1$. (d) $\alpha = 1.1$, $\Delta f = 0.667$, $\rho = 4$.

the threshold region, the loop performance can be characterized by phase error variance. An additional characterization is in terms of bit error probability, P_E, for integrate-and-dump detection of the demodulated output of the loop. Phase error variance and P_E are shown versus ρ in Figs. 10 and 11 for $m = 0.45$ and 0.707, respectively. In contrast to the results given previously for CW interference alone, where phase error variance monotonically decreased with ρ, the results given in Figs. 10 and 11 indicate that for a fixed value of m, an optimum value of ρ exists when Gaussian noise is present in addition to the interference.

Modulated Interference Plus Gaussian Noise

As a somewhat more realistic simulation of a practical situation, results for a modulated interference component, modeled by a narrow-band Gaussian process, plus white Gaussian noise were obtained. To motivate the choice of parameters employed in the simulation, consider the following hypothetical environment, typical of a communica-

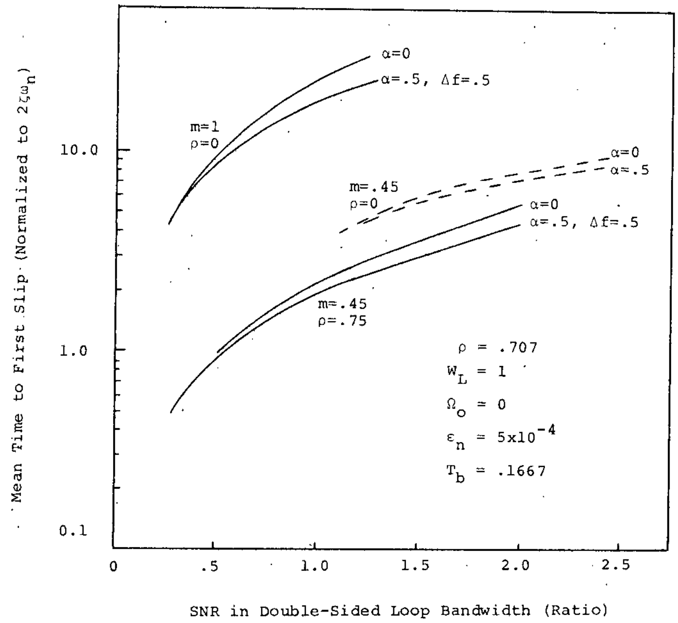

Fig. 9. Normalized mean time to first slip.

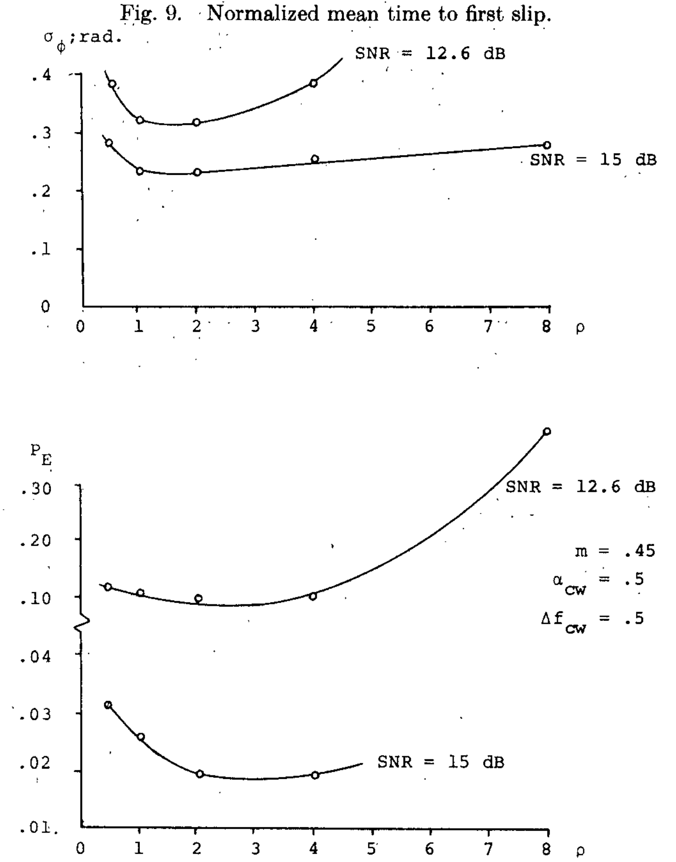

Fig. 10. Phase error standard deviation and P_E for CW RFI plus Gaussian noise; $m = 0.45$.

tions link between a synchronous orbit relay satellite and a low-orbit user satellite or aircraft:

Relay satellite effective radiated power	28 dBw;
Transmit frequency	400 MHz;
Receiver noise temperature	1000 K;
Total system losses	3 dB;
Data rate	1 kbit/s;
Wide-band RFI level (500-km user altitude)	−160 dBm;
Relay-user separation	41 000 km.

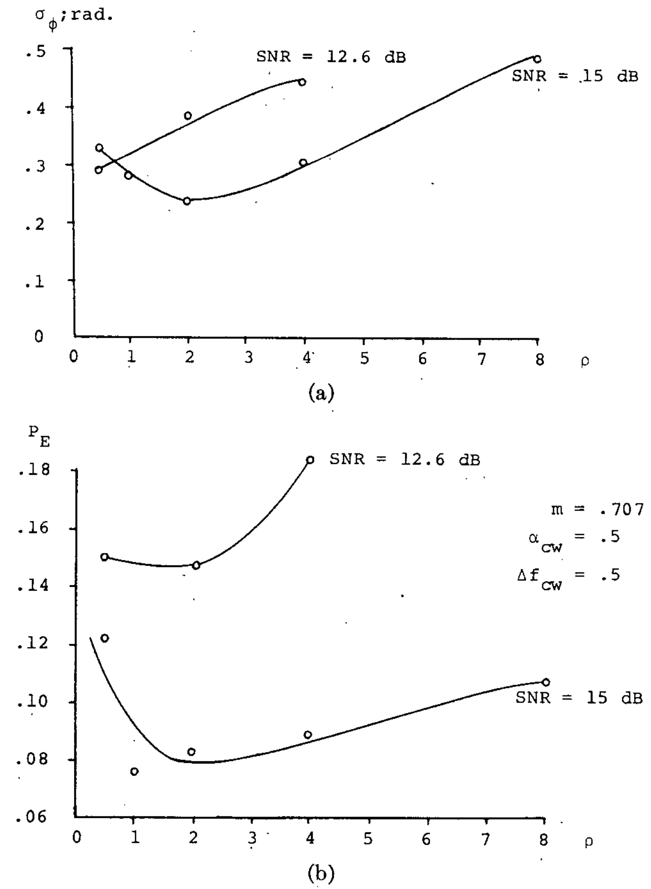

Fig. 11. Phase error standard deviation and P_E for CW RFI plus Gaussian noise; $m = 0.707$.

Assuming an omni-directional antenna on the user, the received signal power is

$$P_R = -152.7 \text{ dBm}.$$

Thermal noise power (2-kHz bandwidth) is

$$P_N = -164.4 \text{ dBw}$$

for a signal-to-noise ratio in a bit-rate bandwidth of

$$\text{SNRBR} = 11.7 \text{ dB}.$$

Assuming the wide-band RFI is uniformly distributed across the signal bandwidth, its level at the receiver is

$$P_T = -157 \text{ dBw}$$

for a signal-to-interference ratio of

$$\text{SNI} = 4.3 \text{ dB}.$$

For simulation purposes suppose that the wide-band RFI is band-limited to the signal bandwidth, but may be offset from the signal carrier by an arbitrary amount (this may not be realistic unless the wide-band RFI is due primarily to a single modulated signal source). The program parameters given in Table I were therefore used in the simula-

TABLE I
PARAMETERS FOR SIMULATION OF A WIDE-BAND RFI ENVIRONMENT

Program Parameter	Meaning	Program Value	Practical System Value
ALPHGI	rms interference-to-signal ratio	0.61 (worst) 0.34 (best)	SNI = 4.3 dB
DELFGI	frequency offset of interference	0.5, 2	100, 400 Hz
WBI	bandwidth of RFI	10 Hz	2000 Hz
SNRWL	signal-to-noise ratio in loop bandwidth	22.5 dB	
T_b^{-1}	bit-rate bandwidth	6 Hz	1200 Hz
B_L	single-sided loop bandwidth	0.5 Hz	100 Hz
Cutoff	cutoff frequency of outer-loop fillers	12 Hz	2400 Hz
Zeta	damping factor	0.707	0.707
AMOD	m	variable	
Rho	ρ	variable	

tion. Corresponding values are also given for a practical system.

Two values of signal-to-interference ratio were used, one corresponding to the worst case link with parameters as given above, and one for an optimistic link for which the effective radiated power is 30 dBw and losses are ignored. The results for the phase error variance are given in Figs. 12 and 13. Again, as in the case of CW RFI plus Gaussian noise, it is apparent that a best choice for ρ exists.

CONCLUSIONS

Results for phase error variance and probability of error for a HT PLL demodulator operating in various combinations of Gaussian noise and RFI backgrounds have been presented. The results of a perturbation analysis for operation in CW RFI compare favorably with the results obtained by digital computer simulations. These results show that a loop which tracks primarily on the modulation component of the signal is preferable in environments consisting of a dominant CW RFI component. The improved performance in CW RFI results because of the averaging by the loop of the (interference) $\times$ (data) component in the loop control voltage, and is most effective for small values of RFI offset frequency compared with the data rate.

When RFI plus noise is present at the loop input, a mode part way between carrier tracking and modulation tracking is preferable due to the importance of (noise) $\times$ (noise) interaction on the phase error in a modulation tracking loop. The results indicate that optimum choices for carrier-to-modulation power and carrier-tracking-loop gain to modulation-tracking-loop gain exist. The same is true for wide-band RFI plus noise backgrounds.

APPENDIX

In this Appendix, the derivation of the loop differential equations (10) are outlined.

For brevity, let the input signal component (4) be written as

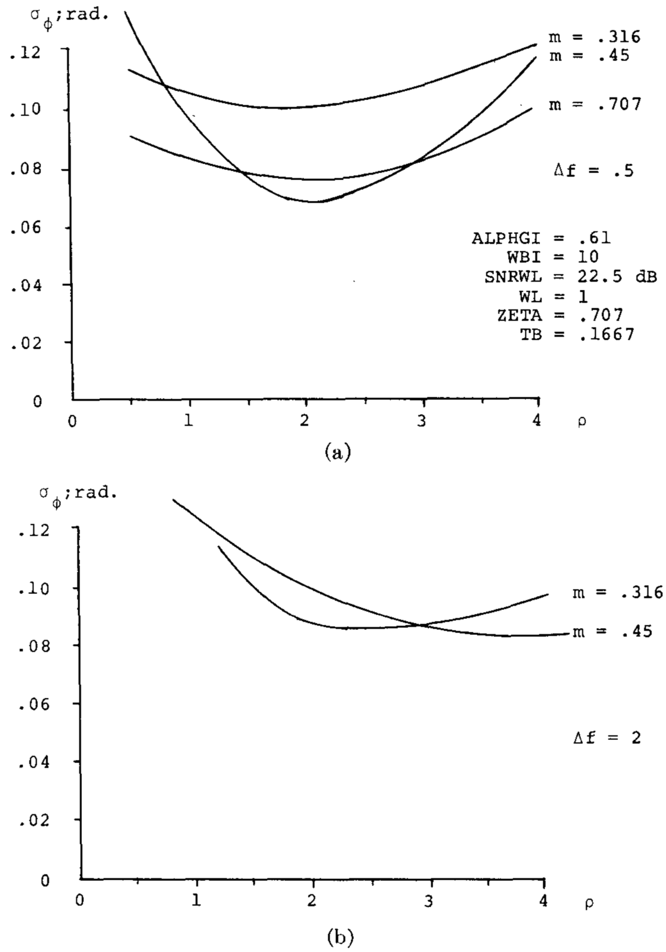

Fig. 12. Phase error standard deviation for modulated RFI plus Gaussian noise. Interference-to-signal ratio = 0.343. (a) Δf = 0.5; (b) Δf = 2.

$$s_k(t) = (2P_c)^{1/2} \sin(\omega_0 t + \theta) + (2S)^{1/2} x_k(t) \cos(\omega_0 t + \theta) \quad \text{(A1)}$$

where $P_c = m^2 P$ is the power in the carrier component and $S = (1 - m^2)P$ is the power in the modulation component. One way of facilitating the separation of the carrier and modulation components within the loop is to place the data $d_k(t)$ on a subcarrier of frequency ω_{sc},

$$x_k(t) = d_k(t) \cos \omega_{sc} t, \quad \text{(A2)}$$

and coherently demodulate it from the subcarrier within the loop as shown in Fig. 1 [1]. A second way is to split phase encode the data as discussed in [2]. We will assume the former method.

Assume that the in-phase and quadrature reference signals generated by the VCO in Fig. 1 are given by

$$r_i(t) = -\sqrt{2} \sin \hat{\Phi}(t) \quad \text{(A3)}$$

and

$$r_q(t) = \sqrt{2} \cos \hat{\Phi}(t), \quad \text{(A4)}$$

respectively, where

$$\hat{\Phi}(t) = \omega_0 t + \hat{\theta}(t) \quad \text{(A5)}$$

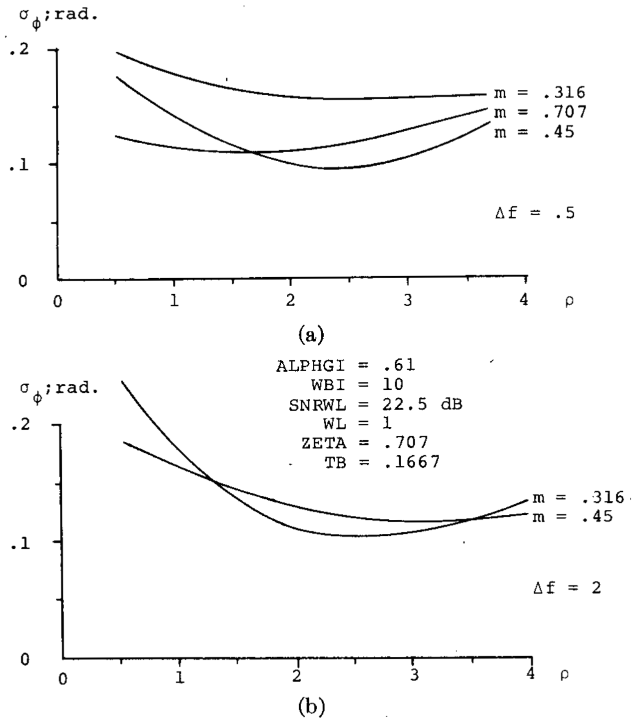

Fig. 13. Phase error standard deviation for modulated RFI plus Gaussian noise. Interference-to-signal ratio = 0.61. (a) $\Delta f = 0.5$; (b) $\Delta f = 2$.

is the loop's estimate of the instantaneous carrier phase of the input signal. Only the difference frequency portions of $Y_2(t)$ and $Y_3(t)$ (see Fig. 1) are of interest since the sum-frequency terms are eliminated by the LPF's. They are

$$Lp[Y_2(t)] = P_c^{1/2} \sin\phi + S^{1/2} x_k(t) \cos\phi + n_c(t) \cos\phi + n_s(t) \sin\phi \quad \text{(A6)}$$

and

$$Lp[Y_3(t)] = -P_c^{1/2} \cos\phi + S^{1/2} x_k(t) \sin\phi + n_c(t) \sin\phi - n_s(t) \cos\phi, \quad \text{(A7)}$$

respectively, where

$$\phi = \Phi - \hat{\Phi} \quad \text{(A8)}$$

is the phase error, and $Lp[\ ]$ denotes the difference frequency part $(\Phi - \hat{\Phi})$ of the signal within the brackets.

With $x_k(t)$ split phase modulated or placed on a subcarrier, the modulation component (second term) of $Lp[Y_2(t)]$ is rejected by the filtering of the closed loop and its effect on loop operation as far as the inner loop is concerned can be ignored. Hence, the effective inner-loop control voltage is

$$Z_1(t) = P_c^{1/2} \sin\phi + n_c(t) \cos\phi + n_s(t) \sin\phi. \quad \text{(A9)}$$

The inputs to the LPF's in the upper and lower legs of the outer loop are $Lp[Y_2(t)]\hat{s}_{sc}(t)$ and $Lp[Y_3(t)]\hat{s}_{sc}(t)$, respectively, where $\hat{s}_{sc}(t)$ is the local subcarrier reference which will be assumed to be perfect here; i.e., there is no timing error present. The filters with transfer function $G(p)$ are chosen to reject all spectral components not at baseband, including the carrier component which appears at $\omega_{sc}/2\pi$ Hz after mixing with the subcarrier, while passing $d_k(t)$ with minimum distortion. The signals $Z_2(t)$ and $Z_3(t)$ may be expressed as

$$Z_2(t) = S^{1/2} d_k(t) \cos\phi + n_1(t) \cos\phi + n_2(t) \sin\phi \quad \text{(A10)}$$

and

$$Z_3(t) = S^{1/2} d_k(t) \sin\phi + n_1(t) \sin\phi - n_2(t) \cos\phi, \quad \text{(A11)}$$

where the noise processes are defined by (16) and (17). Denoting the total loop control voltage by

$$Z_T = F(p)[a_1 Z_1 + a_2 Z_2 Z_3], \quad \text{(A12)}$$

it follows that the instantaneous relative phase, $\hat{\theta}(t)$, of the reference signals, $r_i(t)$ and $r_q(t)$, is governed by the differential equation

$$d\hat{\theta}/dt = k_v Z_T(t) \quad \text{(A13)}$$

where k_v is the VCO constant. In terms of phase error $\phi(t)$, (A13) becomes

$$\frac{d\phi(t)}{dt} = \frac{d\theta(t)}{dt} - k_v Z_T(t). \quad \text{(A14)}$$

Assume the special case of an imperfect second-order loop: $F(p) = (p + a)/(p + \epsilon)$. The loop differential equation without the noise terms then becomes

$$\frac{d\phi}{dt} = \frac{d\theta(t)}{dt} - k_v \frac{p + a}{p + \epsilon}\left[a_1 P_c^{1/2} \sin\phi + a_2 S \frac{\sin 2\phi}{2}\right] \quad \text{(A15)}$$

which, when linearized, can be written as

$$\frac{d^2\phi}{dt^2} + 2\zeta\omega_n \frac{d\phi}{dt} + \omega_n^2 \phi = \frac{d^2\theta}{dt^2} + \epsilon \frac{d\theta}{dt} \quad \text{(A16)}$$

where ζ and ω_n are defined by (7) and (8). Introducing the normalized time variable τ, given by (6), into (A14) results in the equation

$$\dot{\phi}(\tau) = \dot{\theta}(\tau) - \frac{p/(1 + \epsilon_n) + (2\zeta)^{-2}}{p + \epsilon_n/(1 + \epsilon_n)} \frac{F(\tau;\phi)}{m + \rho(1 - m^2)} \quad \text{(A17)}$$

where the dot denotes differentiation by τ and $F(\tau;\phi)$ is given by (12). Letting the state variables be $\phi(\tau)$ and

$$y(\tau) = \frac{\epsilon_n/(1 + \epsilon_n)^2 - (2\zeta)^{-2}}{p + \epsilon_n/(1 + \epsilon_n)} \frac{F(\tau;\phi)}{m + \rho(1 - m^2)}, \quad \text{(A18)}$$

the system of equations denoted as (10) results.

Equation (A17) can be written as a second-order differential equation in standard form as

$$\ddot{\phi}(\tau) + (1 + \epsilon_n)^{-1}\left[\frac{\dot{F}(\tau;\phi)}{m + \rho(1 - m^2)} + \epsilon_n \dot{\phi}(\tau)\right] + (2\zeta)^{-2} \frac{F(\tau;\phi)}{m + \rho(1 - m^2)} = \ddot{\theta}(\tau) + \epsilon_n (1 + \epsilon_n)^{-1} \dot{\theta}(\tau). \quad \text{(A19)}$$

To obtain an expression for $F(\tau;\phi)$ more suitable for analyzing the effects of *cw* RFI, consider (12) with the definitions of Z_1, Z_2, and Z_3 substituted. After considerable simplification by using appropriate trigonometric identities and collecting terms, there results:

$$\begin{aligned} F(\tau;\phi) = {} & m \sin\phi + \tfrac{1}{2}\rho(1-m^2)d_k'^2(\tau)\sin 2\phi \\ & + P^{-1/2}[n_c(\tau)\cos\phi + n_s(\tau)\sin\phi] \\ & + \rho(1-m^2)\{S^{-1/2}d_k'(\tau) \\ & \cdot[n_1(\tau)\sin 2\phi - n_2(\tau)\cos 2\phi] \\ & + \tfrac{1}{2}S^{-1}[n_1^2(\tau) - n_2^2(\tau)]\sin 2\phi \\ & - S^{-1}n_1(\tau)n_2(\tau)\cos 2\phi\}, \end{aligned} \tag{A20}$$

where $d_k'(\tau) = G(p)d_k(\tau)$. Assuming $G(p)$ is chosen such that $d_k'(\tau) \simeq d_k(\tau)$, linearizing the terms involving ϕ alone in (A20), assuming $G(\tau) =$ constant, and substituting into (A19) yields the equation

$$\phi = -H(p')R(\tau,\phi), \tag{A21}$$

where

$$H(p') = \frac{(1+\epsilon_n)^{-1}p' + (2\zeta)^{-2}}{p'^2 + p' + (2\zeta)^{-2}} \tag{A22}$$

$$p' = \frac{d}{d\tau} = \frac{1}{2\zeta\omega_n}\frac{d}{dt} \tag{A23}$$

and

$$R(\tau;\phi) = \frac{F(\tau;\phi) - m\sin\phi + \tfrac{1}{2}\rho(1-m^2)\sin 2\phi}{m + \rho(1-m^2)}. \tag{A24}$$

If (A23) is substituted in (A22) with $\epsilon_n = 0$ (perfect second-order loop) the result is $H(p)$ defined by (25).

To simplify $R(\tau;\phi)$ further, consider the defining relations for $n_1(t)$ and $n_2(t)$, (16) and (17). Working in the t-domain to avoid varying factors of $2\zeta\omega_n$ along, these noise components, assuming *cw* RFI, become

$$n_1(t) = G(p)[2\alpha\cos(\Delta\omega t + \delta)\cos\omega_{sc}t] \tag{A25}$$

and

$$n_2(t) = G(p)[2\alpha\sin(\Delta\omega t + \delta)\cos\omega_{sc}t], \tag{A26}$$

respectively. Using appropriate trigonometric identities and assuming $\Delta\omega \geq 0$, so that $G(p)$ rejects the sum-frequency terms, results in

$$\begin{aligned} n_1(t) = {} & \alpha B(\Delta\omega - \omega_{sc})\cos[(\Delta\omega - \omega_{sc})t - \delta \\ & + \psi(\Delta\omega - \omega_{sc})] \end{aligned} \tag{A27}$$

and

$$\begin{aligned} n_2(t) = {} & \alpha B(\Delta\omega - \omega_{sc})\sin[(\Delta\omega - \omega_{sc})t - \delta \\ & + \psi(\Delta\omega - \omega_{sc})], \end{aligned} \tag{A28}$$

respectively, where (23) has been involved.

Use of (16), (17), (A27), and (A28), along with appropriate trigonometric identities, gives (21) for $R(t;\phi)$.

ACKNOWLEDGMENT

The authors wish to acknowledge the suggestion of Prof. W. C. Lindsey of the University of Southern California that the hybrid loop might possess superior performance characteristics in RFI over conventional loops. The computer programming assistance of Mr. H. R. S. Raghavan is also gratefully acknowledged. Several reviewers' comments aided greatly in improving this paper.

REFERENCES

[1] W. C. Lindsey, "Hybrid carrier and modulation tracking loops," *IEEE Trans. Commun. Technol.*, vol. COM-20, pp. 53–55, Feb. 1972.
[2] T. L. Stewart, "Analysis of a hybrid phase-lock loop," NASA Tech. Note, NASA TN D-5666, June 1970.
[3] T. L. Stewart, "A model for predicting performance of low data rate phase-locked-loop systems," in *Proc. 4th Asilomar Conf. Circuits and Systems*, Dec. 1970, pp. 40–47.
[4] R. E. Ziemer, "Perturbation analysis of the effect of cw interference in Costas loops," in *Conf. Rec., 1972 IEEE Nat. Telemetering Conf.*, Dec. 1972, pp. 20G-1–20G-6.
[5] P. M. Morse and H. Feshback, *Methods of Theoretical Physics.* New York: McGraw-Hill, 1953.
[6] M. J. Levin, "Generation of a sampled time series having a specified correlation function," *IRE Trans. Inform. Theory*, vol. IT-6, pp. 545–548, Dec. 1960.

Rodger E. Ziemer (S'60–M'66–SM'70) was born at Sargeant, Minn., on August 22, 1937. He received the B.S., M.S.E.E., and Ph.D. degrees from the University of Minnesota, Minneapolis, in 1960, 1962, and 1965, respectively.

From 1965 to 1968, he served in active duty with the U. S. Air Force as a First Lieutenant and was engaged in research and development in the areas of aerospace test facility instrumentation and electronic countermeasures. In 1968, he joined the University of Missouri-Rolla, Rolla, where he is currently Professor of Electrical Engineering. His recent research and publications have been concerned with communications through RFI, multipath, and scintillation-fading channels. He has consulted for several companies and government agencies on problems involving communications and radar systems.

Dr. Ziemer is a member of Tau Beta Pi, Eta Kappa Nu, Sigma Xi, and the American Society for Engineering Education.

★

Donald R. Nelson (S'61–M'66) was born in Berwyn, Ill., on October 21, 1940. He received the B.S. degree in electrical engineering from Iowa State University, Ames, in 1962 and the M.S. and Ph.D. degrees in electrical engineering from the University of Missouri-Rolla, Rolla, in 1966 and 1973, respectively.

While at the University of Missouri, he was a member of the Teaching Staff as a Graduate Assistant (1962 to 1963), Instructor (1963 to 1966), and Graduate Teaching Assistant (1969 to 1973). In 1966 he joined the Advanced Development Department of General Dynamics/Electronics, Rochester, N. Y., where he worked on digital TACAN and high-speed wire-line data modems. He is now a member of the Technical Staff in the Department of Computer and Digital Equipment, Aerospace Corporation, El Segundo, Calif.

Dr. Nelson is a member of Phi Eta Sigma, Kappa Mu Epsilon, Eta Kappa Nu, Tau Beta Pi, Phi Kappa Phi, and Sigma Xi.